$HOC_6H_4OCH_2C_6H_4CH_2OC_6H_4OH)(Br(CH_2)_7Br)$ (SRU), 117734-47-1; (4,4′,4″-$HOC_6H_4OCH_2C_6H_4CH_2OC_6H_4OH)(Br(CH_2)_8Br)$ (copolymer), 117734-42-6; (4,4′,4″-$HOC_6H_4OCH_2C_6H_4CH_2OC_6H_4OH)(Br(CH_2)_8Br$ (SRU), 117734-48-2; (4,4′,4″-$HOC_6H_4OCH_2C_6H_4CH_2OC_6H_4OH)(Br(CH_2)_9Br)$ (copolymer), 117734-43-7; (4,4′,4″-$HOC_6H_4OCH_2C_6H_4CH_2OC_6H_4OH)(Br(CH_2)_9Br)$ (SRU), 117734-49-3; (4,4′,4″-$HOC_6H_4OCH_2C_6H_4CH_2OC_6H_4OH)(Br(CH_2)_{10}Br)$ (copolymer), 117734-44-8; (4,4′,4″-$HOC_6H_4OCH_2C_6H_4CH_2OC_6H_4OH)(Br(CH_2)_{10}Br)$ (SRU), 117734-50-6; (4,4′,4″-$HOC_6H_4OCH_2C_6H_4CH_2OC_6H_4OH)(Br(CH_2)_{11}Br)$ (copolymer), 117734-45-9; (4,4′,4″-$HOC_6H_4OCH_2C_6H_4CH_2OC_6H_4OH)(Br(CH_2)_{11}Br)$ (SRU), 117734-51-7; (4,4′,4″-$HOC_6H_4OCH_2C_6H_4CH_2OC_6H_4OH)(Br(CH_2)_{12}Br)$ (copolymer), 117734-46-0; (4,4′,4″-$HOC_6H_4OCH_2C_6H_4CH_2OC_6H_4OH)(Br(CH_2)_{12}Br)$ (SRU), 117734-52-8; α,α′-diphenoxy-*p*-xylene, 10403-79-9; α,α′-dibromo-*p*-xylene, 623-24-5; phenol, 108-95-2; bis(4-hydroxyphenoxy)-*p*-xylene, 108196-53-8; 1,10-bis(4-hydroxyphenoxy)decane, 70856-53-0; hydroquinone, 123-31-9; sodium hydroxide, 1310-73-2; tetrabutylammonium bromide, 1643-19-2.

References and Notes

(1) Flory, P. J. *Proc. R. Soc. London* **1956**, *Ser. A234*, 73.
(2) de Gennes, P.-G. *C. R. Seances Acad. Sci.* **1975**, *Ser 281B*, 101.
(3) Roviello, A.; Sirigu, A. *J. Polym. Sci., Polym. Lett. Ed.* **1975**, *13*, 455.
(4) Ober, C. K.; Jin, J.-I.; Lenz, R. W. *Adv. Polym. Sci.* **1984**, *59*, 103.
(5) Shaffer, T. D.; Percec, V. *Makromol. Chem., Rapid Commun.* **1985**, *6*, 97.
(6) Blumstein, A.; Sivaramakrishnan, K.; Clough, S. B.; Blumstein, R. B. *Mol. Cryst. Liq. Cryst. Lett.* **1979**, *49*, 255.
(7) Shaffer, T. D.; Percec, V. *J. Polym. Sci., Polym. Lett. Ed.* **1985**, *23*, 185.
(8) Iimura, K.; Koido, N.; Okta, R.; Takeda, M. *Macromol. Chem.* **1981**, *182*, 2563.
(9) Roviello, A.; Sirigu, A. *Makromol. Chem.* **1979**, *180*, 2543.
(10) Percec, V.; Shaffer, T. D.; Nava, H. *J. Polym. Sci., Polym. Lett. Ed.* **1984**, *22*, 637.
(11) Flory, P. J. *Adv. Polym. Sci.* **1984**, *59*, 2.
(12) Chung, T.-S. *Polym. Eng. Sci.* **1986**, *26*, 901.
(13) Ericsson, J.; Hult, A. *Polym. Bull.* **1987**, *18*, 295.
(14) Johansson, K. E.; Palm, T.; Werner, P.-E. *J. Phys. E., Sci. Instrum.* **1980**, *13*, 1289.
(15) Griffin, A. C.; Havens, S. J. *J. Polym. Sci., Polym. Phys. Ed.* **1981**, *19*, 951.
(16) N'Guyen, T. D.; Boileau, S. *Polym. Bull.* **1979**, *1*, 817.
(17) Cameron, G. G.; Law, K. S. *Makromol. Chem., Rapid Commun.* **1982**, *3*, 99.
(18) Yamazaki, N.; Imai, Y. *Polym. J.* **1983**, *15*, 603.
(19) Percec, V.; Auman, B. C. *Makromol. Chem.* **1984**, *185*, 617.
(20) Yamazaki, N.; Imai, Y. *Polym. J.* **1985**, *17*, 377.
(21) Percec, V.; Nava, H.; Jonsson, H. *J. Polym. Sci., Part A: Polym. Chem.* **1987**, *25*, 1943.
(22) Percec, V.; Nava, H. *J. Polym. Sci., Part A: Polym. Chem.* **1987**, *25*, 405.
(23) Shaffer, T. D.; Jamaludin, M.; Percec, V. *J. Polym. Sci., Polym. Chem. Ed.* **1985**, *23*, 2913.
(24) Cox, J. D.; Pilcher, G. *Thermochemistry of Organic and Organometallic Compounds*; Academic Press: London, 1970.
(25) Benson, S. *J. Chem. Educ.* **1965**, *42*, 502.
(26) Griffin, A. C.; Havens, S. J. *J. Polym. Sci., Polym. Lett. Ed.* **1980**, *18*, 259.
(27) Krigbaum, W. R.; Watanabe, J.; Isikawa, T. *Macromolecules* **1983**, *16*, 1271.
(28) Abe, A. *Macromolecules* **1984**, *17*, 2280.
(29) Yoon, D. Y.; Bruckner, S. *Macromolecules* **1985**, *18*, 651.
(30) Demus, D.; Richter, L. *Textures of Liquid Crystals*; VEB Deutscher Verlag für Grundstoffindustrie: Leipzig, 1978.

First-Order Wetting Transitions of Polymer Mixtures in Contact with a Wall

I. Carmesin

Institut für Physik, Universität Mainz, Postfach 3980, Max-Planck-Institut für Polymerforschung, Mainz, Federal Republic of Germany

J. Noolandi*

Xerox Research Centre of Canada, 2660 Speakman Drive, Mississauga, Ontario L5K 2L1, Canada.
 Received June 23, 1988

ABSTRACT: A binary mixture of polymers A and B in contact with a wall C is considered at coexistence. The system is isotropic in two directions and inhomogeneous in the direction d perpendicular to the surface. We study the polymer profiles within a selected range of two parameters, namely, the local chemical potential at the surface μ_1 and a parameter g which controls the strength of the attractivity of the surface. In order to study the system we carry out a mean-field self-consistent calculation of the polymer distribution functions, based on the biased diffusion equation, to account for the polymer–polymer and polymer–wall interaction energies, as well as the changes in the conformational and configurational entropies due to the presence of the surface. For the range of parameters considered, we find strong first-order wetting transitions. The limitations of the long-wavelength approximation to surface problems, developed earlier, are pointed out.

1. Introduction

A polymer mixture in contact with a wall at coexistence of both the A-rich and the B-rich phases shows wetting transitions depending on the interaction of polymers A and B with the wall. This means that a macroscopically thick layer at the wall can be found experimentally depending on the temperature, the chain length, the kind of polymers, and the nature of the surface. Theoretically the interaction of the polymers with the surface has been described by the local chemical potential μ_1 and a second parameter g controlling the attractivity of the surface.[1] One of us has earlier analyzed this problem in the long-wavelength limit of the Flory–Huggins approximation and found first-order wetting, critical wetting, and tricritical wetting.[2] This approach breaks down if one looks at the problem at low bulk concentration (here "bulk" means far away from the wall) of one of the components.[3] In this paper we make use of a more general mean-field approach starting from the functional integral representation for a polymer mixture, which does not suffer from the above limitation.[4,5] Comparing the results of the more general theory, we find that under certain conditions, in which we get strong

0024-9297/89/2222-1689$01.50/0 © 1989 American Chemical Society

first-order wetting transitions, the long-wavelength approximation may be used to get a rough estimate of parameters describing the interactions of the polymers with the surface. This consequence shuld be useful for an analysis of experiments currently in progress.[6] As in the previous work,[2] we assume, for simplicity, that the system is isotropic parallel to the surface of the wall.

In section 2 we review the long-wavelength approximation and describe in detail the biased diffusion equation for the polymer distribution functions, as well as the associated free energy, of the functional integral approach for polymer mixtures perturbed by the presence of an interacting surface. In addition we rationalize our choice of the interaction energy of polymers A and B with the wall. In section 3 we present the results of the calculation, and in the last section we give a short summary.

2. Theory

2a. Description of Wetting Transitions in the Long-Wavelength Approximation ($k \to 0$). We describe the polymer mixture by the usual Flory–Huggins approach.[1,3,7] In addition to the usual terms for a binary mixture we have additional terms for the interaction of polymers A and B with the wall. We write for the free energy of mixing[1,2]

$$\Delta F/k_BT = \int d^3r \left\{ \frac{b^2}{36\phi(1+\phi)}(\nabla\phi)^2 + \frac{\phi}{Z}\ln\phi + \frac{(1-\phi)}{Z}\ln(1-\phi) + \chi\phi(1-\phi) + (\mu_1\phi + {}^1\!/_2 g\phi^2)\delta(x) \right\} \tag{2-1}$$

where x is the direction perpendicular to the surface, ϕ is the volume fraction of polymer A, and $1-\phi$ is the volume fraction of polymer B for the two-component system. The degrees of polymerization of the polymers are Z_A, Z_B (we assume Z_A, $Z_B = Z$ above) and the Kuhn length is b for both A and B. $\chi_{AB} = \chi$ is the Flory–Huggins interaction parameter, μ_1 the local chemical potential at the surface, and g a second parameter describing the interaction of the polymers with the surface.

As one can see the bare free energy at the surface (the term proportional to $\delta(x)$) derives from a Taylor series expansion. This ansatz is described more explicitly in ref 2 and is the standard approach to surface problems in statistical mechanics.[8] Depending on the signs, μ_1 and g describe reflecting, adsorbing, or repulsive surfaces. Minimizing ΔF in the bulk and at the surface and requiring continuity of the concentration profiles give the relations from which the phase portrait diagram can be derived, as shown in Figure 1 (intersection of two curves described by eq 2-2 and 2-3)

$$\frac{b^2}{18\phi(1-\phi)}\left.\frac{\partial\phi}{\partial x}\right|_{x=0} = -\mu_1 - g\phi|_{x=0} \tag{2-2}$$

$$\frac{b^2}{18\phi(1-\phi)}\left.\frac{\partial\phi}{\partial x}\right|_{x=0} = \pm\frac{b}{3}\left[\frac{G(\phi,\chi) - G(\phi_\infty,\chi)}{\phi(1-\phi)}\right]^{1/2}\Bigg|_{x=0} \tag{2-3}$$

with

$$G(\phi,\chi) = \frac{1}{Z}\{\phi\ln\phi + (1-\phi)\ln(1-\phi) + \chi Z\phi(1-\phi)\} \tag{2-4}$$

The intersection points in Figure 1 are possible surface concentrations ϕ_1; in this calculation the bulk concentration ϕ_∞ is fixed. Note that only $\phi_1^{(1)}$, $\phi_1^{(3)}$ correspond to possible local minima of the free energy. $\phi_1^{(2)}$ always corresponds to a local maximum. We can now distinguish a number of different cases.

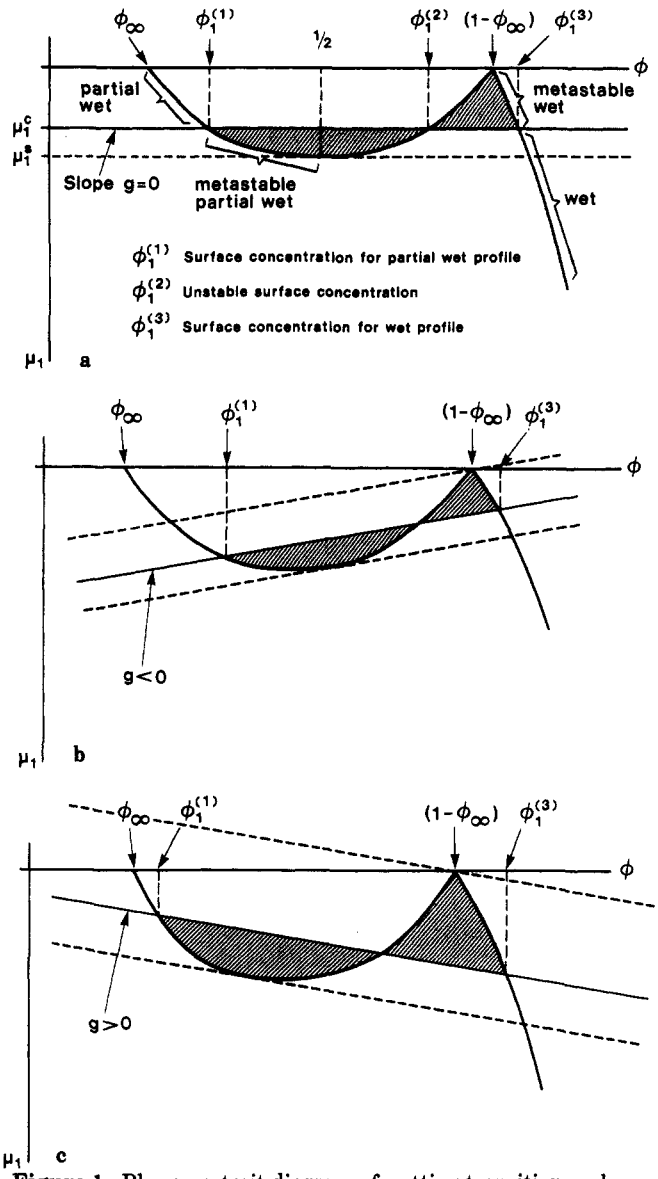

Figure 1. Phase portrait diagram of wetting transitions, where ϕ_∞, $1-\phi_\infty$ are the volume fractions of polymers A and B in the bulk, respectively. The phase transition is found if the two hatched areas are equal. By increasing μ_1 (g = constant), one can reach the wet state from a partial wet state with small μ_1. The left crossing point $\phi_1^{(1)}$ is the surface concentration in the partial wet case; the right crossing point for the wet case is $\phi_1^{(3)}$. (a) $g = 0$; (b) $g < 0$; in the latter case there exists a second-order phase transition if $|g|$ is large enough, corresponding to no discontinuity between $\phi_1^{(1)}$ and $\phi_1^{(3)}$. (c) For $g > 0$ there is a strong first-order transition, corresponding to the large discontinuity between $\phi_1^{(1)}$ and $\phi_1^{(3)}$. The value of μ_1 at the spinodal point is μ_1^s.

In Figure 1a the slope of the straight line is zero. $\phi_1^{(1)}$, $\phi_1^{(3)}$ are the possible stable solutions depending on μ_1. If the two hatched areas are equal, the phase transition between the partial wet ($\phi_1^{(1)} < 1-\phi_\infty$) and the wet state ($\phi_1^{(3)} > 1-\phi_\infty$) takes place at $\mu_1 = \mu_1^c$. There is a discontinuity in the surface concentration ($\phi_1^{(3)} - \phi_1^{(1)}$) corresponding to a first-order transition. If $\mu_1 < \mu_1^c$, $\phi_1^{(1)}$ is the stable surface concentration corresponding to the partial wet state, and $\phi_1^{(3)} > 1-\phi_\infty$ is the surface concentration of the metastable wet solution. If $\mu_1 > \mu_1^c$, $\phi_1^{(3)}$ is the stable surface concentration for the wet state and $\phi_1^{(1)}$ is the metastable surface concentration for the partial wet state (for μ_1 less than the value of the local chemical potential at the spinodal point $\mu_1 = \mu_1^s$).

In Figure 1b the parameter g is <0; $|g|$ is the slope of the straight line. In this case we have the same features as described above. In addition here we can distinguish between first- and second-order transitions and a tricritical point in between. The tricritical point is defined by $|g| = |g^c|$ and $\phi_1^{(1)} = \phi_1^{(3)} = 1 - \phi_\infty$, where $|g^c|$ is the slope of the curve at a concentration $1 - \phi_\infty$. In this case the surface concentration is also equal to $1 - \phi_\infty$. For $|g| > |g^c|$ there exists only one solution, there is no discontinuity in the surface concentrations if we vary μ_1 and we find only second-order transitions. For $|g| < |g^c|$ there are first-order transitions as for $g = 0$.

In Figure 1c the parameter g is >0. Here we find the same feature as shown in Figure 1a, and we have a large discontinuity $\phi_1^{(3)} - \phi_1^{(1)}$ at the phase transition, corresponding to a strong first-order phase transition. The dashed lines indicate the surface spinodals.

2b. Description of a Polymer Mixture by the Functional-Integral Approach. In this part we describe the polymer mixture in the self-consistent mean-field approximation, which reduces to the previous approach in the long-wavelength limit. For completeness we repeat some of the basic results; a detailed description can be found elsewhere.[5]

The number of polymer chains of type p is denoted by $\tilde{N}_p = N_p/Z_p$, where N_p is the number of monomer units and Z_p is the degree of polymerization. The partition function then reads

$$\mathbf{Z} = \left\{\prod_p \frac{(Z_{\text{kin}})^{\tilde{N}_p}}{\tilde{N}_p!}\right\} \int \{\prod_p \prod_{j=1}^{\tilde{N}_p} \mathcal{D}\{\mathbf{r}_{pj}(\cdot)\} P[\mathbf{r}_{pj}(\cdot)] \exp(-\beta V)\} \tag{2-5}$$

where Z_{kin} is the partition function due to the kinetic energy and βV is the interaction energy of polymer A, polymer B, and the wall multiplied by $\beta = (k_B T)^{-1}$. The index j runs over all the molecules of type p. The integral is over all space curves $\mathbf{r}(\cdot)$, which represents possible configurations of the macromolecules and is denoted by $\int \mathcal{D}\{\mathbf{r}_{pj}(\cdot)\}$. The probability density functional for a given space curve is given by $P[\mathbf{r}_{pj}(\cdot)]$ and assumed to be of standard Wiener form, i.e.

$$P[\mathbf{r}_{pj}(\cdot)] \propto \exp\left[-\frac{3}{2b^2}\int_0^{Z_p} dt\, \mathbf{r}_{pj}(\cdot)\right] \tag{2-6}$$

b being the Kuhn statistical length of a single segment of the polymer, assumed to be the same for polymers A and B in this case.

Using the integral representation of the δ function and writing out the intermolecular potential explicitly in terms of all the space curves, we can recast eq 2-5 as follows:

$$\mathbf{Z} = \mathcal{N} \int \{[\prod_p \mathcal{D}\rho_p(\cdot)\mathcal{D}\omega_p(\cdot)] \exp(-F[\{\rho_p(\cdot)\},\{\omega_p(\cdot)\}])\} \tag{2-7}$$

with the microscopic density operator defined by

$$\rho_p(\mathbf{r}) = \sum_{j=1}^{N_p} \int_0^{Z_p} dt\, \delta[\mathbf{r} - \mathbf{r}_{pj}(t)] \tag{2-8}$$

and $\mathcal{N}$ a normalization constant. F is the free energy functional, given by

$$F[\{\rho_p(\cdot)\},\{\omega_p(\cdot)\}] = W[\{\rho_p(\cdot)\}] - \sum_p \int d^3r\, \omega_p(\mathbf{r})\rho_p(\mathbf{r}) + \sum_p \int d^3r\, \frac{\rho_p(\mathbf{r})}{Z_p}\left\{\ln\left[\frac{N_p}{Z_p Z_{\text{kin}} \mathbf{Q}_p}\right] - 1\right\} \tag{2-9}$$

Note that the combinatorial term in front of the partition function gives rise to the last term in eq 2-9, through the use of Stirling's approximation, and represents the configurational entropy of the polymer molecules. The second term in eq 2-9 arises from the integral representation of the δ function and accounts for conformational entropy changes of the polymers, once the mean-field potential is defined by the minimization of the free energy. W is the total interaction energy divided by $k_B T$ and the quantity $\mathbf{Q}_p$ is given by

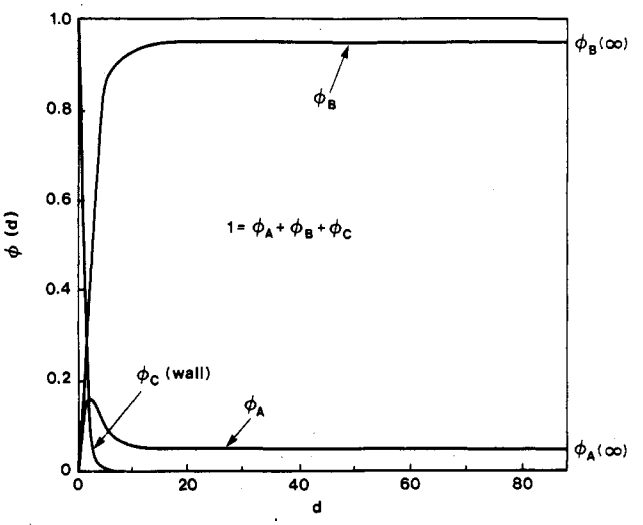

Figure 2. Typical profiles for polymer A (ϕ_A), polymer B (ϕ_B), and ϕ_C representing the wall, as a function of the distance d from the wall. $d = d_{\max}$ (in terms of the Kuhn length b) corresponds to the bulk.

$$\mathbf{Q}_p = \int \delta\mathbf{r}(\cdot) P[\mathbf{r}_p(\cdot)] \exp\left\{-\int_0^{Z_p} dt\, \omega_p[\mathbf{r}(t)]\right\} = \int d^3r \int d^3r_0\, Q_p(\mathbf{r},Z_p|\mathbf{r}_0) = \int d^3r\, q_p(\mathbf{r},t) \tag{2-10}$$

The function $Q_p(\mathbf{r},t|\mathbf{r}_0)$ is the primary quantity of interest, representing the unnormalized distribution function for a chain with t segments, starting at $\mathbf{r}_0$ and ending at $\mathbf{r}$, and can be shown to satisfy the modified diffusion equation

$$\frac{\partial}{\partial t} Q_p = \frac{b^2}{6}\nabla^2 Q_p - \omega_p Q_p \tag{2-11}$$

The quantity ω_p is the mean-field function which leads to a distortion of the random walk conformation of a polymer chain of type p according to the local environment of the polymer chain. In order to obtain an expression for ω_p we must minimize the functional F subject to the following constraints: (i) the incompressibility of the mixture, or no volume change *locally* upon mixing

$$\sum_p [\rho_p(\mathbf{r})/\rho_{0p}] = \sum_p \phi_p(\mathbf{r}) = 1 \tag{2-12}$$

where ρ_{0p} is the density of pure polymer in monomer segments per unit volume, and (ii) a constant number of particles

$$\int d^3r\, \rho_p(\mathbf{r}) = N_p \tag{2-13}$$

In order to carry out the free energy minimization by the saddle-function method with the above constraints, we introduce two Lagrangian multipliers $\eta(\mathbf{r})$ and λ_p and obtain the variational equations

$$\omega_p = \frac{\partial W}{\partial \rho_p} + \frac{\eta(r)}{\rho_{0p}} - \lambda_p \tag{2-14}$$

$$\rho_p(\mathbf{r}) + \frac{N_p}{\mathbf{Q}_p}\frac{\delta Q_p}{\delta \omega_p(\mathbf{r})} = 0 \tag{2-15}$$

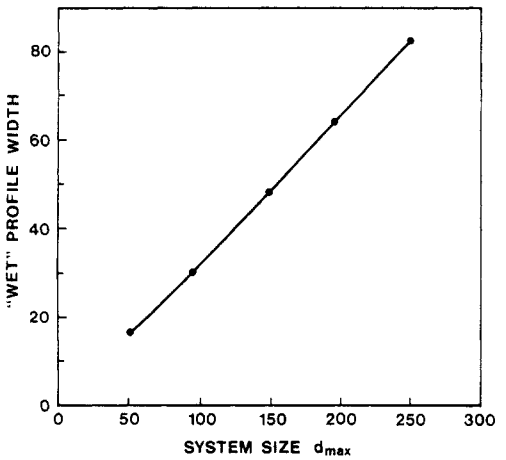

Figure 3. Width of the wet profile is plotted against size of the system (in terms of the Kuhn length b). This graph also shows the range of system sizes for which the calculations in the paper were carried out. The width shows a linear dependence on the system size, as expected for finite dimensions.

Equation 2-14 gives the expression for the mean-field ω_p, and the density $\rho_p(\mathbf{r})$ is found from eq 2-15

$$\rho_p(\mathbf{r}) = \frac{N_p}{Z_p \mathbf{Q}_p} \int_0^{Z_p} dt\; q_p(\mathbf{r},t) q_p(\mathbf{r},Z_p-t) \qquad (2\text{-}16)$$

The quantity $\mathbf{Q}_p$ can be chosen so that $\mathbf{Q}_p = N_p/\rho_{0p}$, thus converting eq 2-16 into a relation for the volume fraction $\phi_p(\mathbf{r})$, with a prefactor of $1/Z_p$ in front of the integral. Note that this expression does not reduce to the often quoted form $\rho_p(\mathbf{r}) \propto q_p^2$ except in the limit of infinite molecular weight, when the distribution function becomes independent of the curvilinear parameter t. Equation 2-14 expresses the constancy of the chemical potential, and as shown in ref 5, the quantity λ_p can be eliminated from this expression, making use of the fact that the mean field is a constant in the bulk homogeneous phase. This point is illustrated in section 2d, where explicit expressions for the mean fields of polymers A and B are given. The above equations must be solved self-consistently, and this procedure is described in the Appendix. However the contributions due to the interaction of the polymers with the surface have to be included in the total interaction energy W. In the following we discuss the form of this surface interaction and reduce our problem to one dimension, retaining only the direction d perpendicular to the surface. The system is assumed to be isotropic in the other two directions.

2c. Explicit Description of the Interaction with a Wall and Comparison with the $k \to 0$ Approximation. We describe the wall by a *fixed* profile $\phi_c(d)$, where d is the direction perpendicular to the wall, which is equal to unity at the wall ($d = 0$) and falls rapidly to zero within a few Kuhn lengths as shown in Figure 2. The profile $\phi_c(d)$ is fixed throughout the entire calculation and not

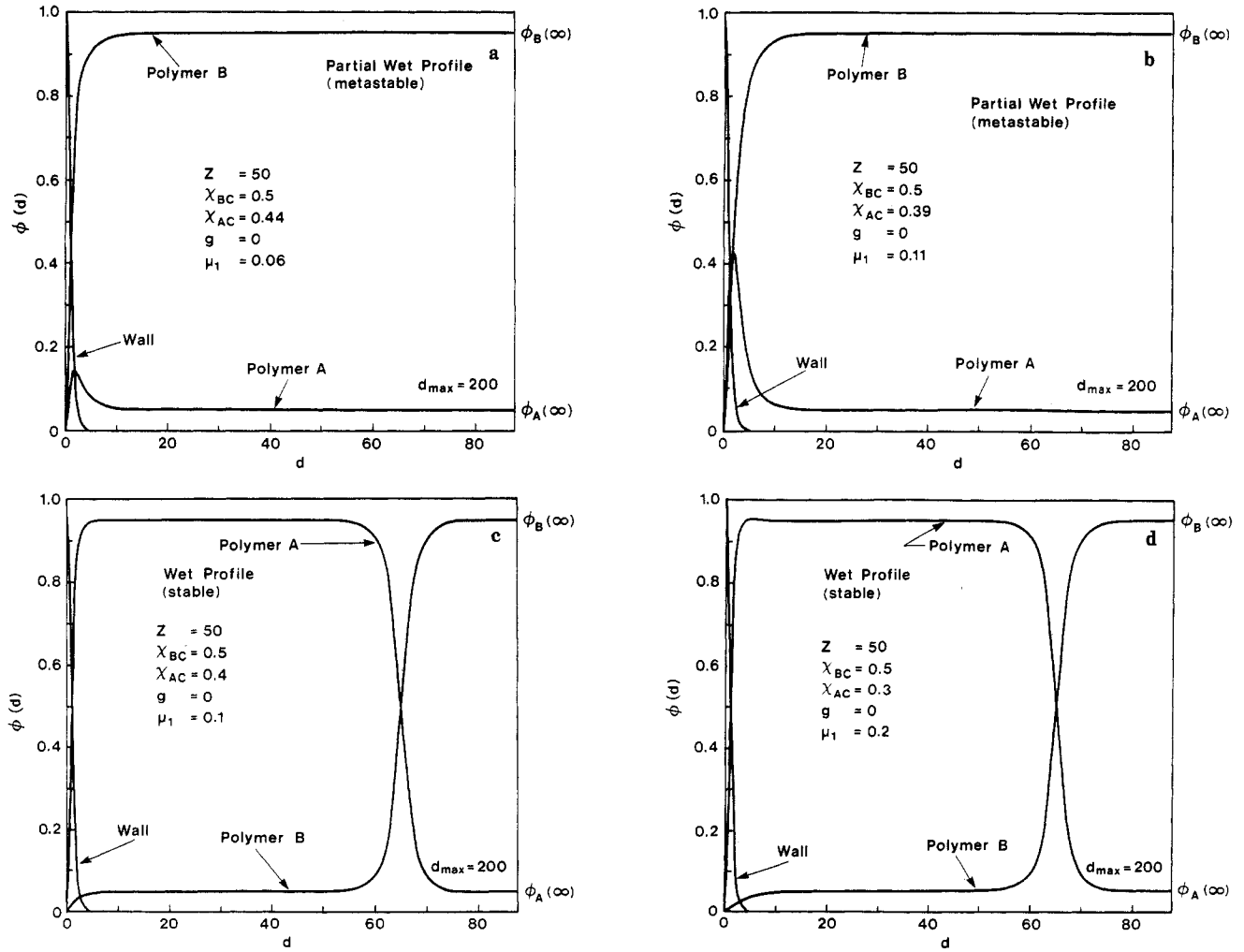

Figure 4. Calculated concentration profiles of polymers A, B with $\mu_1 = \chi_{BC} - \chi_{AC} - g$: (a) metastable partial wet profile, with $g = 0$, $\mu_1 < \mu_1^c$; (b) metastable partial wet profile, $g = 0$, $\mu_1 > \mu_1^c$; (c) stable wet profile (near the phase transition), $g = 0$, $\mu_1 \geq \mu_1^c$; (d) stable wet profile, $g = 0$, $\mu_1 > \mu_1^c$. The polymer density profile calculations were carried out with constant χ_{BC} and varying χ_{AC}, constant degree of polymerization Z, $d_{max} = 200$ (the system size in terms of the Kuhn length b), and $\phi_A(\infty) = 0.05$.

directly involved in the minimization process mentioned earlier. It is given by

$$\phi_c(d) = 1 - \tanh^2 (ad/b) \quad (2\text{-}17)$$

where a is a numerical constant and b is the Kuhn length. In the calculations we choose $a = 1.75$ for convenience. The results of the calculations are not sensitive to the specific value of a, provided the wall profile falls sharply to zero within a few Kuhn lengths of the "bulk" surface. ϕ_c then depends only on d, the direction perpendicular to the wall. There are also nonadditive microscopic interactions (including the effects of "missing" neighboring molecules) between the wall and polymers A and B, giving rise to terms in the free energy density (quantified by the parameter g) in addition to those describing polymer–wall contact interactions through Flory–Huggins interaction parameters ($\chi_{\text{polymer-wall}}$)

$$f^{\text{bare}}_{\text{surface}} = \chi_{AC}\phi_A\phi_C + \chi_{BC}\phi_B\phi_C - \tfrac{1}{2}g\phi_C(\phi_A^2 + \phi_B^2) \quad (2\text{-}18)$$

where ϕ_A, ϕ_B are the volume fractions (concentrations) of polymers A and B. The incompressibility conditions has been used to reduce the different nonadditive interaction parameters (g_{AA}, g_{BB}, g_{AB}) into the one independent quantity denoted by g. The superscript "bare" refers to enthalpic interactions with the wall alone. The more complicated entropic contributions to the free energy will be discussed in section 2d. Equation 2-18 can be rewritten, again using the condition of incompressibility near the surface, $1 = \phi_A + \phi_B + \phi_C$ (for all d)

$$f^{\text{bare}}_{\text{surface}} = (\chi_{AC} - \chi_{BC} + g)\phi_C\phi_A - g\phi_C\phi_A^2 + \text{constant terms} \quad (2\text{-}19)$$

In order to compare with the quantities used in the long-wavelength limit ($k \to 0$), one has to integrate the free energy density $f^{\text{bare}}_{\text{surface}}$

$$\begin{aligned} F^{\text{bare}}_{\text{surface}} &= \int_0^\infty dx\, f^{\text{bare}}_{\text{surface}} \\ &= \int_0^\infty dx\, [[\chi_{AC}\phi_A + \chi_{BC}\phi_B]\phi_C - \tfrac{1}{2}g\phi_C(\phi_A^2 + \phi_B^2)] \\ &= \int_0^{d_{\max}} dx\, [(\chi_{AC} - \chi_{BC} + g)\phi_C\phi_A - g\phi_C\phi_A^2] + \text{constant terms} \\ &\approx (\chi_{AC} - \chi_{BC} + g)\phi_{A1} - g\phi_{1A}^2 + \text{constant terms} \end{aligned} \quad (2\text{-}20)$$

The surface concentration is defined by

$$\phi_{1A} = \int_0^{d_{\max}} dx\, \phi_C\phi_A \approx \int_0^{\zeta_c} dx\, \phi_C\phi_A \approx \phi_A(\zeta_c) \quad (2\text{-}21)$$

where ζ_c is the distance from the surface where ϕ_c ($d = \zeta_c$) has fallen to a value smaller than 10^{-3}. Note that we have not taken the maximum of $\phi_A(d)$ (see Figure 2) in order to define the surface concentration ϕ_{1A} but have chosen instead $\phi_A(\zeta_c)$. The reason for this is that in the two cases the interaction with the surface is described differently. In one case, in the $k \to 0$ limit we have a δ-function interaction and in the other case we have a "wall profile" $\phi_c \neq 0$ with a length scale ζ_c. The condition of incompressibility $\phi_A + \phi_B = 1$ for the two polymers alone holds only for $d > \zeta_c$. There is a certain arbitrariness in the definition of ϕ_{1A} in this description; however, we have discussed this point only for the purpose of making contact with the long-wavelength approximation. The free energy curves shown in section 3 were all obtained by precise numerical integration of the full free energy density expression (including the interaction terms given by eq 2-18) discussed in section 2d.

In the long-wavelength limit $f^{\text{bare}}_{\text{surface}}$ can also be written as a series expansion in the surface concentration, since near the tricritical point [where $\phi_{1A} \approx 1 - \phi_A(\infty)$] $(1 - \phi_{1A})$ is a small quantity (because we assume $\phi_A(\infty)$ is small), giving

$$\begin{aligned} f^{\text{bare}}_{\text{surface}}(k\to 0) &= \mu_1(k\to 0)(1 - \phi_{1A}) - \tfrac{1}{2}g(k\to 0)(1 - \phi_{1A})^2 + \text{constant terms} = \\ &-[\mu_1(k\to 0) - g(k\to 0)]\phi_{1A} - \tfrac{1}{2}g(k\to 0)\phi_{1A}^2 + \text{constant terms} = -\mu_1\phi_{1A} - \tfrac{1}{2}g(k\to 0)\phi_{1A}^2 + \text{constant terms} \end{aligned} \quad (2\text{-}22)$$

Here $\mu_1(k\to 0)$ is the appropriate interaction parameter if we expand $f^{\text{bare}}_{\text{surface}}$ in $(1 - \phi_{1A})$, and μ_1 is the corresponding parameter if we write $f^{\text{bare}}_{\text{surface}}$ as a series in ϕ_{1A}, with $\mu_1 = \mu_1(k\to 0) - g(k\to 0)$.

Comparing (2-20) and (2-22) we conclude that for polymeric interactions with the wall the connection between the two descriptions can be established by assuming

$$\mu_1 = \chi_{BC} - \chi_{AC} - g \quad (2\text{-}23)$$

$$g(k\to 0) = 2g \quad (2\text{-}24)$$

Note that although there are two Flory–Huggins-type surface parameters, χ_{AC} and χ_{AB}, in the theory, the result depends only on their difference $(\chi_{AC} - \chi_{AB})$.

2d. Expressions for the Mean Fields and the Total Free Energy. Simplifying the expression for the total free energy, using eq 2-9 and 2-14, we can now write

$$F = \sum_p \mu_p N_p + F_{\text{surface}} A \quad (2\text{-}25)$$

where μ_p is the chemical potential in the bulk, F_{surface} is the total surface free energy per unit area, and A is the area of the surface. The explicit expression for F_{surface} is, following the derivation given in an earlier paper[5]

$$\begin{aligned} F_{\text{surface}} = \rho_0 \int_0^\infty dx \Bigg\{ &-\frac{[\eta(x) - \eta(\infty)][1 - \phi_c(x)]}{\rho_0} - \\ &\frac{1}{Z_A}[\phi_A(x) - \phi_A(\infty)] - \frac{1}{Z_B}[\phi_B(x) - \phi_B(\infty)] - \\ &\chi_{AB}[\phi_A(x)\phi_B(x) - \phi_A(\infty)\phi_B(\infty)] - f^{\text{bare}}_{\text{surface}}(x) \Bigg\} \end{aligned} \quad (2\text{-}26)$$

where $f^{\text{bare}}_{\text{surface}}(x)$ is given by eq 2-18. The term $[1 - \phi_c(x)]$ provides the convergence required in the free energy density at $x = 0$, since $\Delta\eta/\rho_0$ diverges to infinity as x approaches the wall. The Lagrangian multiplier λ_p in eq 2-14 has been eliminated by referring the mean fields to their constant values in the bulk phase. The corresponding explicit expressions for the mean fields are

$$\omega_A(x) = -\frac{1}{Z_A}\ln \phi_A(\infty) + \chi_{AB}[\phi_B(x) - \phi_B(\infty)] - g\phi_C(x)\phi_A(x) + \chi_{AC}\phi_C(x) + \frac{\Delta\eta}{\rho_0} \quad (2\text{-}27)$$

$$\omega_B(x) = -\frac{1}{Z_B}\ln \phi_B(\infty) + \chi_{AB}[\phi_A(x) - \phi_A(\infty)] - g\phi_C(x)\phi_B(x) + \chi_{BC}\phi_C(x) + \frac{\Delta\eta}{\rho_0} \quad (2\text{-}28)$$

where $\Delta\eta = \eta(x) - \eta(\infty)$ and we have used the relations $\omega_A(\infty) = -(1/Z_A)\ln \phi_A(\infty)$ and $\omega_B(\infty) = -(1/Z_B)\ln \phi_B(\infty)$ for the bulk phase. The quantity $\Delta\eta/\rho_0$ is an unknown function which must be determined entirely from the self-consistency condition for the solution of the two coupled differential equations for the probability distri-

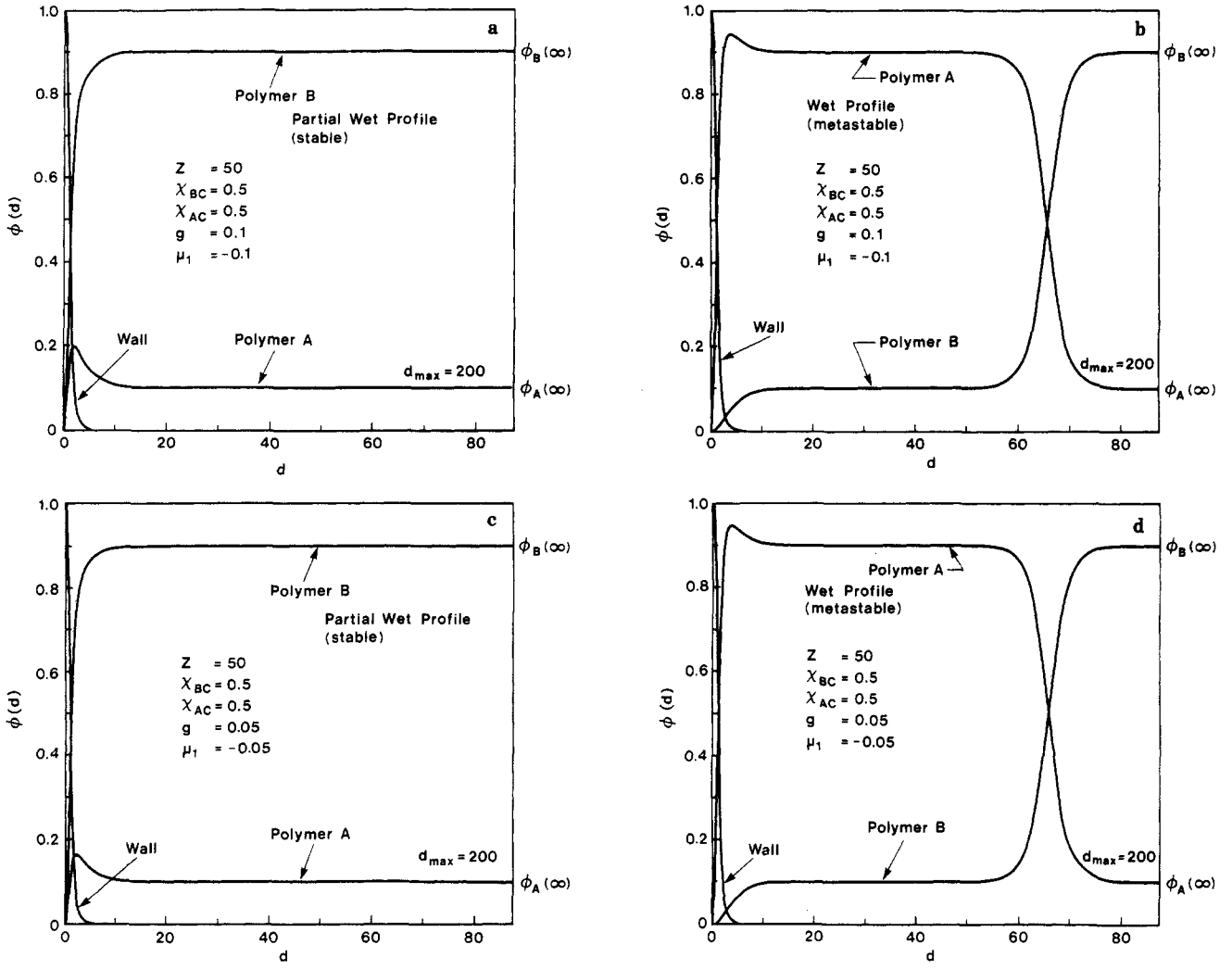

Figure 5. Stable partial wet (a) and metastable wet (b) profiles corresponding to the starred points on the free energy diagram in Figure 6a with $\mu_1 = -0.01$. (c, d) The stable partial wet and metastable wet profiles, respectively, corresponding to the solid dots in Figure 6a, with $\mu_1 = -0.05$.

bution functions of polymers A and B. This important problem is discussed in the Appendix.

Note that the entire surface free energy includes configurational and conformational entropy terms which are related to changes in the polymer density profiles in a highly nonlinear way, as well as the polymer interactions with the wall ($F^{bare}_{surface}$) and modifications of the extent of polymer–polymer interactions themselves near the wall. Note also that, although the polymer–wall interaction energy depends only on the difference $\chi_{BC} - \chi_{AC}$, the same is not true for the mean-field potentials individually.

Finally, since we are always on the coexistence curve, the interaction parameter χ_{AB} is given by

$$\chi_{AB} = \frac{\ln [\phi_A(\infty)/\phi_B(\infty)]}{Z[\phi_A(\infty) - \phi_B(\infty)]} \qquad (2\text{-}29)$$

where $Z_A = Z_B = Z$.

3. Results

The calculations of the polymer profiles shown in this paper were all carried out on a system of size $d_{max} = 200b$, where b is the Kuhn length. Profiles representing the wet state show a plateau at a high concentration $1 - \phi_\infty$ of one component, if ϕ_∞ is the low bulk concentration of the same component. The thickness of the wet layer (where the flip-over from ϕ_∞ to $1 - \phi_\infty$ occurs and which corresponds to the A-rich phase if the bulk is a B-rich phase as in our case) is always around 32% of d_{max}. The thickness of the surface layer in the wet case scales with the finite system size as shown in Figure 3. For an infinite system the layer itself would be infinite as the interface between the preferred phase near the wall and the bulk phase gets "depinned" from the wall and a macroscopic "wetting layer" forms.

We have carried out all calculations with a bulk concentration $\phi_A(\infty)$ in the range 0.01–0.2. In the following figures calculations are shown for $\phi_A(\infty) = 0.05, 0.1$, with chain lengths up to $200b$. Although we have included both parameters χ_{AC} and χ_{AB} in the theory, the results depend only on the difference $\chi_{BC} - \chi_{AC}$, as expected. For all parameters investigated we found first-order wetting transitions for large enough μ_1. In Figure 4 typical profiles are shown for a degree of polymerization $Z = 50$, a bulk concentration $\phi_A(\infty) = 0.05$, with different local chemical potentials μ_1 and constant $g = 0$. One clearly sees in Figure 4a,b profiles for the partial wet state. The concentration ϕ_{1A} at the surface is a little higher than the bulk concentration. With increasing μ_1 the surface concentration increases, but the state shown in Figure 4b is metastable, because its free energy is higher than that of the wet state with the same surface parameters. In Figure 4c,d the profiles for the wet state are shown. The plateau described above is also clearly seen. The profiles in Figure 4 correspond to a first-order phase transition depending on μ_1. The order parameter for this transition is the inverse thickness of the wetting layer $1/l$, which is zero in an

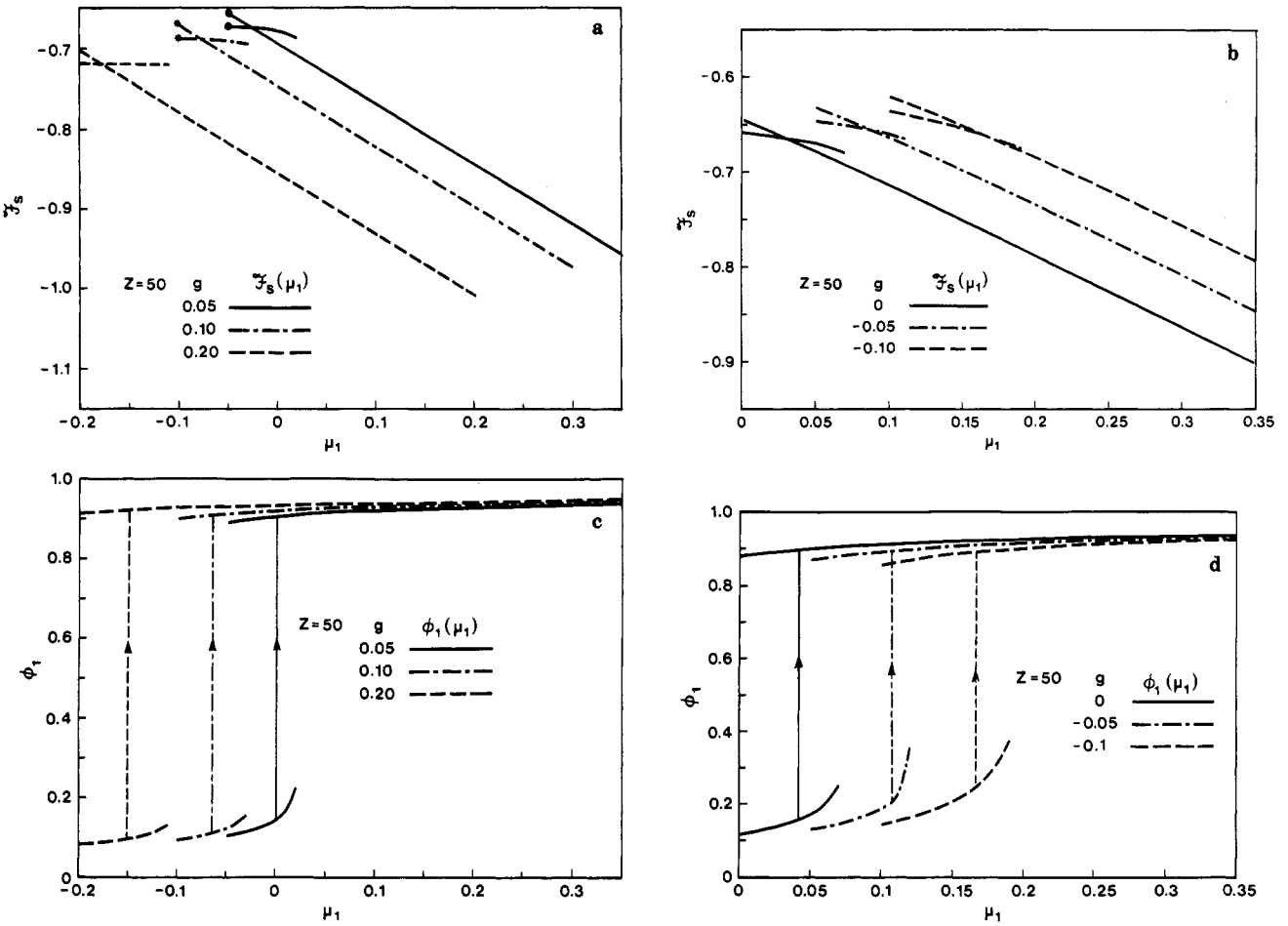

Figure 6. Surface free energy calculations showing first-order phase transitions. (a, b) Surface free energy plotted versus the local chemical potential μ_1. In the metastable region two branches exist. The branch with the lower free energy corresponds to the stable state, and the crossing points correspond to the phase transition. (c, d) The surface-concentrations corresponding to Figures 6a,b are plotted versus the local chemical potential. The straight lines indicate the phase transition, given by the crossing points in Figure 6a,b.

infinite system in the wet state. Here we clearly see a discontinuity of $1/l$ at the transition point.

For $g \neq 0$ we find similar features. Here examples are shown for $\phi_A(\infty) = 0.1$ and μ_1 constant. In Figure 5 both stable partial wet profiles and metastable wet profiles are shown. The two kinds of numerically stable solutions are obtained from the numerical algorithm outlined in the Appendix. The metastable solutions found here are typical for first-order phase transitions. As shown in Figure 6a,b for the surface free energy $F_s(\mu_1)$, for a given value of g two branches of the free energy are found, belonging to the wet and the partial wet states. With increasing values of g we get stronger first-order phase transitions as the angle between the two branches at the crossing point increases in Figure 6a, also shown more clearly in Figure 6b. The analogous result for the surface concentration is shown in Figure 6c,d, where the discontinuities of the surface concentrations are shown. With decreasing positive values of g (Figure 6c) and more negative g (Figure 6d), the discontinuities become smaller. In all these cases there exists a broad region of the wet metastable state. The two asterixs in Figure 6a correspond to the profiles shown in Figure 5a,b and also indicate the points where the calculations were chosen to be discontinued. Similarly the two solid dots in Figure 6a correspond to the profiles in Figure 5c,d. It is difficult to define numerically the limits of metastability for both branches, because we cannot distinguish whether the numerical method eventually breaks down or the region of metastability does not exist. In Figure 6c,d it is also seen that ϕ_1[partial wet] $\equiv \phi_1^{(1)}$ varies rapidly with μ_1, but ϕ_1[wet] $\equiv \phi_1^{(3)}$ is almost constant with μ_1. The same kind of behavior is found in the long-wavelength approximation.[2]

As shown in Figure 7, the phase-transition point is shifted to smaller values of μ_1 as the chain length increases. This behavior is also in qualitative agreement with the long-wavelength theory (compare with eq 2-2 and 2-3). In Figure 8 the full calculation and the results from the long-wavelength limit are compared directly. The parameters are transformed as shown in section 2. We see that the transition points found within the long-wavelength approximation lie at lower μ_1; however, both calculations agree qualitatively for this region of parameter space, in the range of first-order phase transitions. We find a much smaller region of metastable wet profiles in the long-wavelength approximation, and a simple scaling of the parameters cannot explain this difference. In our current work we did not specifically study tricritical wetting and second-order phase transitions. However, the long-wavelength theory predicts second-order phase transitions for large negative g. In this work we find a trend to weaker first-order transitions if g decreases, in agreement with the results in the $k \to 0$ limit.

4. Conclusions

We have shown that within the mean-field self-consistent approach, first-order wetting transitions exist and there is qualitative agreement with the long-wavelength approximation over the limited range of surface interaction parameters (μ_1,g) studied. Therefore it may be possible

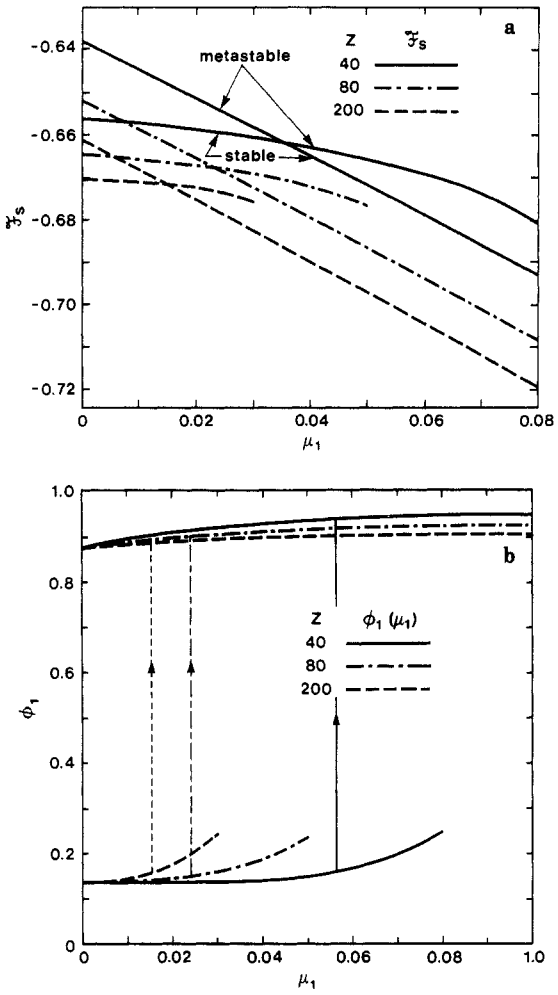

Figure 7. First-order phase transitions are shown for varying chain lengths, with $g = 0$, showing (a) surface free energy versus μ_1 and (b) surface concentration versus μ_1.

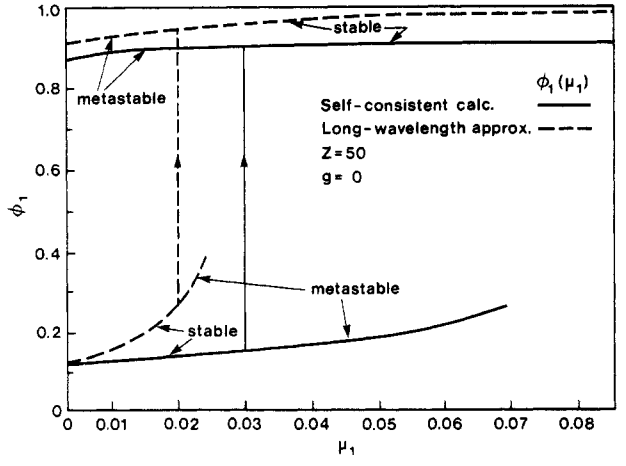

Figure 8. Comparison of the first-order wetting transitions found in the self-consistent calculations studied in this paper and the long-wavelength approximation studied in earlier work, making use of the relationship between the interaction parameters discussed in section 2c.

to use the long wavelength approximation if the bulk concentration $\phi_A(\infty)$ is not too small (clearly this approximation breaks down in the limit $\phi_A(\infty) \to 0$). Moreover this is the first instance where it has been demonstrated that the mean-field self-consistent approach can be effectively implemented to study a multi-length-scale phenomenon such as wetting, where the Kuhn length b, the degree of polymerization of the polymer molecules Z, the system size d_{max}, and the length ζ_c (describing the wall) are all included. The wet state is seen very clearly in our work. Our efforts in this direction should be useful for a more extended study of the details of the overall polymer phase diagram, including wetting phenomena. By expending more effort on improving the numerical accuracy, this class of problems can be studied with even lower bulk polymer concentrations and larger absolute values of g. In this case one could carry out a detailed study of the tricritical point. Also it should be possible to carry out calculations in the one-phase region and not only on the coexistence curve, as we have restricted ourselves. These extended calculations may be more realistic for the various experiments or surfaces in contact with polymer blends which are currently in progress. One such promising experimental approach uses the technique of forward recoil spectroscopy.[6] Rapid advances in numerical analysis for nonlinear theoretical problems, and significant increases in computing power, coupled with novel experimental techniques and instrumentation, should enable a detailed microscopic understanding of polymer–surface interactions for both scientific and technological purposes.

Acknowledgment. We thank L. M. Marks for developing the computer programs used to evaluate the polymer density profiles and the surface free energies and Professor K. Binder for initial correspondence and discussions relating to this work.

Appendix

Here we discuss the procedure for solving the diffusion equation

$$q_t = q_{xx} - \omega q \tag{A-1}$$

for the polymer distribution functions q_A, q_B, with the appropriate mean-field potentials ω_A, ω_B given by eq 2-27 and 2-28. Since these potentials are coupled in a highly nonlinear fashion and moreover involve the determination of an unknown function $\Delta\eta(x)/\rho_0$, the self-consistent solution of diffusion equations is the most difficult and ill-posed part of our study of wetting transitions near a wall.

For the numerical solution of eq A-1, we use a nonlinear grid of sampled data points $[x(i)]$ near the wall

$$x(i) = \left\{\frac{\exp(\gamma t_i) - 1}{\exp(\gamma) - 1}\right\} d_{max} \tag{A-2}$$

where $t_i = (i - 1)/200$, $i = 1, ..., 200$, $3 < \gamma < 5$, and d_{max} is the system size (in terms of the Kuhn length). This choice of the grid heavily weights the density of data points near the wall, where most of the variation of the polymer density profiles takes place.

The general idea behind the numerical procedure is as follows: since we do not know the function $\omega_A(x)$, we make the first guess $\omega_A(x) \simeq \omega_A(\infty)$. Then we solve the partial differential equation (A-1) for $q_A(x,t)$ with the initial conditions and boundary conditions

$$q_A(x,0) = 1 \qquad q_A(0,t) = 0, \quad t > 0 \tag{A-3}$$

using the Crank-Nicolson method[9] with the nonlinear grid given by eq A-2. The volume fraction $\phi_A(x)$ is then determined from the convolution integral

$$\phi_A(x) = \int_0^1 q_A(x,s) q_A(x,t-s)\, ds \tag{A-4}$$

where the upper limit of the integral has been scaled so that s runs from 0 to 1, with $ds = \Delta s = 0.005$.

Now the incompressibility condition gives

$$\phi_B(x) = 1 - \phi_C(x) - \phi_A(x) \tag{A-5}$$

where $\phi_C(x)$ is the preassigned wall profile, defined by eq 2-17. We also have, from the definitions of $\omega_A(x)$ and $\omega_B(x)$

$$\omega_B(x) = \omega_A(x) - g\phi_C(x)[\phi_B(x) - \phi_A(x)] - [\omega_A(\infty) - \omega_B(\infty)] - (\chi_{AC} - \chi_{BC})\phi_C(x) - \chi_{AB}[\phi_B(x) - \phi_A(x) + \phi_A(\infty) - \phi_B(\infty)] \quad \text{(A-6)}$$

Next we solve eq A-1 for polymer B using eq A-5 and A-6 to get the estimates $q'_B(x,t)$, $\phi'_B(x)$. At this point it is convenient to define

$$\frac{\Delta\eta(x)}{\rho_0} = \tfrac{1}{2}\{\omega_A(x) - \omega_A(\infty) + \omega_B(x) - \omega_B(\infty) + (\chi_{AB} - \chi_{AC} - \chi_{BC})\phi_C(x) + g\phi_C(x)[\phi_A(x) + \phi'_B(x)]\} \quad \text{(A-7)}$$

and

$$\phi'_A(x) = 1 - \phi_C(x) - \phi'_B(x) \quad \text{(A-8)}$$

Then we use the quantities $\Delta\eta(x)/\rho_0$, $\phi_A(x)$, $\phi'_B(x)$ in eq 2-27 to obtain $\omega'_A(x)$. It follows, after some algebra, that

$$\omega'_A(x) - \omega_A(x) = \left(\chi_{AB} + \frac{g\phi_C}{2}\right)(\phi'_B - \phi_B) \quad \text{(A-9)}$$

so if $\omega'_A(x) \to \omega_A(x)$, this implies that $\phi'_B(x) \to \phi_B(x)$ and $\phi'_A(x) \to \phi_A(x)$. We want $\omega'_A(x) - \omega_A(x)$ to vanish for all x, but it is sufficient to use $x = x(i)$. This difference, computed at $x = x(i)$, is a functional vector depending on the independent vector $\omega_A(x)$. Note that $\omega'_A(x)$, a vector derived from $\omega_A(x)$, is *not* the next guess for $\omega_A(x)$. The next estimate of $\omega_A(x)$ (to get $\omega'_A(x)$ to converge to $\omega_A(x)$) requires a procedure to solve a nonlinear system of (vector) equations in an unknown vector $[\omega_A(x)]$. For our problem we use the generalized secant method.[10]

References and Notes

(1) Cahn, J. W. *J. Chem. Phys.* **1977**, *66*, 3667. Nakanishi, H.; Pincus, P. *J. Chem. Phys.* **1983**, *79*, 997.
(2) Schmidt, I.; Binder, K. *J. Phys.* **1985**, *46*, 1631–1644.
(3) Binder, K. *J. Chem. Phys.* **1983**, *79*, 6387; *Phys. Rev. A* **1984**, *29*, 341.
(4) Helfand, E. *J. Chem. Phys.* **1975**, *62*, 999.
(5) Hong, K. M.; Noolandi, J. *Macromolecules* **1981**, *14*, 727.
(6) Kramer, E. Unpublished results.
(7) de Gennes, P.-G. *J. Chem. Phys.* **1980**, *72*, 4756. Pincus, P. *J. Chem. Phys.* **1981**, *75*, 1996.
(8) Binder, K. Critical Behavior at Surfaces. In *Phase Transitions and Critical Phenomena*; Domb, C., Lebowitz, J., Eds.; Academic Press: New York, 1984; Vol. 8 and references therein.
(9) Fox, L. *Numerical Solution of Ordinary and Partial Differential Equations*; Addison-Wesley: Reading, MA, 1962.
(10) Wolfe, P. *Commun. ACM* **1959**, *2*, 12.

Ultrasound-Mediated Reductive Condensation Synthesis of Silicon–Silicon Bonded Network Polymers

Patricia A. Bianconi,† Frederic C. Schilling, and Timothy W. Weidman*

AT&T Bell Laboratories, Murray Hill, New Jersey 07974.

Received June 3, 1988; Revised Manuscript Received September 29, 1988

ABSTRACT: The synthesis of the first poly(alkylsilynes), $(RSi)_n$, a new class of silicon–silicon bonded network materials, has been accomplished by using high-intensity ultrasound to mediate a "virtually homogeneous" reduction of alkylsilicon trichlorides with liquid NaK alloy emulsions. This procedure provides good control over reaction kinetics and stoichiometry by promoting instantaneous initiation and quantitative reaction of the reductant under mild conditions and prevents the premature separation of incompletely reduced polymer. The new polymers $(RSi)_n$ (with R = alkyl > two carbons and $n < 1000$) remain soluble in nonpolar organic solvents, from which they can readily be cast into transparent yellow amorphous films. All chemical and spectroscopic data indicate that polysilynes are constructed primarily of sp^3-hybridized alkylsilicon units assembled into irregular networks that exhibit extensive Si–Si σ-delocalization.

Introduction

Polysilanes, linear polymers possessing an all silicon–silicon bonded backbone, have recently been shown to exhibit a variety of interesting properties and applications that have stimulated extensive research efforts.[1-7] The first example of these materials, poly(dimethylsilane), was described by Burkhard in 1949 as an intractable white powder[3] but received little attention until 1975, when Yajima reported that it could be converted to fibers of β-SiC.[4] The development that accelerated the pace of polysilane research to its current state was the report by West and co-workers of a soluble polysilane, a 1:1 copolymer of dimethylsilane and phenylmethylsilane.[5] While formally analogous to saturated polyolefins, polysilanes typically exhibit an intense near-UV absorption, the position of which shifts with changes in molecular weight and in response to factors affecting the conformation of the polymer backbone.[6] Both the electronic spectra and photochemistry of polysilanes are now generally interpreted by invoking the delocalization of both Si–Si bonding and close-lying antibonding states along the polymer backbone.[1h] Upon irradiation, efficient photofragmentation occurs with extrusion of both silylenes (R_2Si:) and cyclic oligomers, a property which has led to their evaluation as positive photoresists for microelectronics.[7] The intrinsically high silicon content of these polymers is an additional advantage in this application since the unexposed polymer may be converted into SiO_2 by oxygen ion etching.

Although linear polysilanes bearing an impressive diversity of alkyl, aryl, and even trimethylsilyl substituents[8] have now been prepared and investigated, there has been little progress toward the preparation and characterization of monoalkyl silicon polymers, $(RSi)_n$.[9] By direct analogy to carbon-based polymers, materials with a 1:1 alkyl to silicon ratio could adopt either discrete aromatic structures or take the form of linear conjugated polymers analogous to polyacetylenes. Alternatively, and more consistent with the decreased tendency of silicon toward π-bonding, a network structure with no carbon analogue may be adopted. In either case, such materials, viewed as the halfway point between polysilanes and silicon, should exhibit an intriguing array of physical properties.

† Current address: Department of Chemistry, 152 Davey Laboratory, Pennsylvania State University, University Park, PA 16802.

0024-9297/89/2222-1697$01.50/0

© 1989 American Chemical Society